The generality of the standard 2D TFM approach in predicting bubbling fluidized bed hydrodynamics

Schalk Cloete[1], Abdelghafour Zaabout[2], Stein Tore Johansen[2], Martin van Sint Annaland[3], Fausto Gallucci[3] & Shahriar Amini[2]

1) Norwegian University of Science and Technology (NTNU), Norway

2) SINTEF Materials and Chemistry, Norway

3) Technical University of Eindhoven (TU/e), the Netherlands

1 Abstract

Hydrodynamic simulations of a pseudo-2D bubbling fluidized bed were carried out and compared to experiments conducted over a wide range of flow conditions. The primary purpose of this study was to assess the generality of the standard 2D Two Fluid Model (TFM) closed by the Kinetic Theory of Granular Flows (KTGF) which is regularly used in the literature to simulate bubbling fluidized beds. Comparisons of the bed expansion ratio over wide ranges of fluidization velocity, bed loading and particle size showed systematic differences between simulations and experiments, indicating that the generality of this modelling approach is questionable. More detailed flow velocity measurements collected via Particle Image Velocimetry (PIV) showed that the model greatly over-predicts flow velocities in the bed. Subsequent 3D simulations showed this over-prediction to be the result of 2D simulations neglecting the wall friction at the front and back walls of the pseudo-2D bed.

2 List of symbols

2.1 Main Symbol definitions

α	Volume fraction
ϕ	Kinetic energy transfer rate (kg/m.s^3)
γ	Dissipation rate (kg/m.s^3)
Θ_s	Granular temperature (m^2/s^2)
ρ	Density (kg/m^2)
ς	Specularity coefficient
$\bar{\bar{\tau}}$	Stress tensor (kg/m.s^2)
$\vec{\tau}_s$	Particle shear force at the wall (N)
$\vec{\upsilon}$	Velocity vector (m/s)
∇	Del operator / Gradient (1/m)
d	Diameter (m)
$\vec{g}$	Gravity vector (m/s^2)

$g_{0,ss}$	Radial distribution function
H	Bed height (m)
$\bar{\bar{I}}$	Identity tensor
K	Momentum exchange coefficient (kg/(m^3.s)
k	Diffusion coefficient (kg/m.s)
p	Pressure (Pa)
t	Time (s)
$\vec{U}_{s,\|\|}$	Particle velocity parallel to wall (m/s)

2.2 Sub- and superscript definitions:

0	Initial/static
Θ_s	Granular temperature
$\exp$	Experiment
g	Gas
gs	Inter-phase
$\max$	Maximum packing
s	Solids
sim	Simulation

2.3 Abbreviations

ANOVA	Analysis of variance
by	Interaction effect
CCD	Charge-coupled device
CFD	Computational fluid dynamics
d	Particle diameter
H	Initial static bed height
KTGF	Kinetic theory of granular flows
L	Linear effect
LED	Light emitting diode
PIV/DIA	Particle image velocimetry combined with digital image analysis
Q	Quadratic effect
RMS	Root mean square
SS	Sum of squares
TFM	Two fluid model
U	Fluidization velocity

3 Introduction

Since the kinetic theory of granular flows (KTGF) [1, 2] was first proposed three decades ago, fundamental hydrodynamic simulations of bubbling fluidized beds have been regularly carried out within the research community. Naturally, validation efforts soon followed to show that the two fluid model (TFM) closed by the KTGF could give reasonable representations of reality even though only relatively coarse 2D grids were affordable at the time.

As computational power increased, finer meshes could be employed and validation studies against lab-scale physical models could be completed in 2D [3-8] and in 3D [9, 10] with less numerical uncertainties. In general, results were encouraging, but rarely achieved a completely satisfactory match. The primary source of uncertainty quoted lies in the formulation of the various closure models incorporated into the KTGF.

Despite numerous uncertainties still remaining in terms of hydrodynamic modelling, significant research efforts have recently been invested in extending the KTGF to reactive flows [11-15]. Incorporation of chemical reactions significantly increases the complexity of the system due to the close coupling between hydrodynamics and chemical kinetics [16] and, due to this close coupling, predictions of overall reactor performance are highly dependent on accurate simulation of the underlying hydrodynamics.

Studies attempting to validate reactive fluidized bed simulations are rare and limited by the lack of sufficiently detailed or generic experimental data. One study completed on a chemical looping combustion system found that a 2D TFM KTGF approach could not reproduce a counter-intuitive experimental trend extracted over a range of fluidization velocities [15]. The qualitative failure of the numerical model drew attention to the sensitivity of reactive fluidized bed systems and the unexpected non-linear effects that can become highly influential. In this case, the fine length scales at the gas inlet together with the 2D assumption were responsible for the discrepancy. Inaccuracies in the hydrodynamic response of the model to changes in the fluidization velocity therefore led to a reactive fluidized bed model that was not generally applicable.

Generality is the ultimate aim of any fundamental predictive model. If the model is used to meet aims such as prototyping, design, optimization and scale-up, adequate generality is implicitly assumed since the model will inevitably be used to simulate conditions far removed from those under which it was validated. A model responding incorrectly to changes in any one of the multitude of design and operating variables defining a fluidized bed reactor (such as the example given in the previous paragraph) can therefore lead to dangerously erroneous conclusions.

When considering the importance of generality in the field of simulation based engineering, it is surprising that the vast majority of validation studies are focussed on one or a very limited number of flow situations. After all, adequate validation in a single case, even when completed in great detail, is no guarantee of generality throughout the parameter space defined by the numerous flow variables involved.

Recent work completed on different modelling strategies for fluidized bed reactors [17, 18] identified clear systematic discrepancies between 1D, 2D and 3D modelling approaches within a parameter space defined by fluidization velocity, reactor temperature, solids loading and particle size. Although trends were predicted to be qualitatively similar, quantitative discrepancies tended to constantly increase with changes in certain flow variables. These works therefore showed the importance of defining any systematic differences between model and experiment before attempting to use such a model for purposes of simulation based engineering. If the model cannot be made to be fully generic, fixed boundaries on its range of applicability at least have to be determined.

For this reason, a thorough and systematic validation campaign is required to evaluate the performance of various fluidized bed reactor models with a specific focus on generality. Care should also be taken to structure the validation studies in such a way that the four primary sets of physical phenomena –

hydrodynamics, species transfer, heat transfer and reaction kinetics – are decoupled so as to avoid non-linear coupled effects which hinder the useful interpretation of data.

The present work is the first step in such a campaign. It will evaluate the hydrodynamic generality of the widely used 2D TFM KTGF approach to simulating bubbling fluidization over a wide range of fluidization velocities, solids loadings and particle sizes.

The paper first gives an overview of the experimental, simulation and data processing methods employed. Results are then presented in the form a grid independence study, a generality study, some visual qualitative comparisons between simulations and experiments and some more detailed solids velocity comparisons. Finally, some conclusions are drawn from the results.

4 Experiments

4.1 Experimental set up

The experimental setup (Figure 1) consisted of a pseudo-2D fluidized bed column with a height of 1.5 m, a width of 0.3 m and a depth of 0.015 m. The front plate of the column was made from glass to allow for visual access to the bed as required by the experimental technique used in this study (Particle Image Velocimetry combined with Digital Image Analysis - PIV/DIA). A metallic black plate was used at the back in order to reduce light reflections when recording images.

A porous plate with 40 µm average pore size and 3 mm thickness was used as the gas distributor. Mass flow controllers were used to control the gas inlet flow rate and the column was equipped with an expanding metallic freeboard at the top in order to prevent elutriation of fine particles at higher flowrates.

Humidified air was used to fluidize spherical glass beads with a density of 2500 kg/m^3. Five different particle size distributions were studied: 70-110, 100-200, 200-300, 300-400 & 400-600 µm. More details about the size distributions are given in Table 1.

Table 1: Particle size distribution of the different particle sizes investigated in this study.

Particle range (µm)	70-110	100-200	200-300	300-400	400-600
D10 (µm)	80	135	220	300	430
D50 (µm)	95	170	270	360	478
D90 (µm)	115	200	310	420	526

A high speed CCD camera (Lavision model Image Pro HS4M) was used to film the bed from the front for two purposes: determining the expanded bed height by means of image analysis and determining the particle velocity field based on PIV/DIA. Lighting was supplied by four LED lamps.

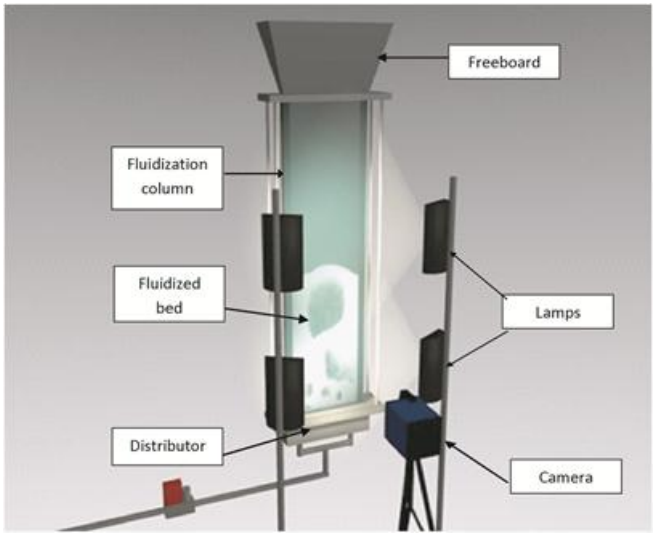

Figure 1: Schematic representation of the experimental set up.

4.2 Particle image velocimetry

PIV is a non-invasive optical measurement technique that determines the particle velocity from two images recorded in short succession. The two images are analysed by first dividing each image into N×N interrogation areas and then applying a cross correlation to determine the average particle displacement in each interrogation area.

As recommended in a previous study [19], the filmed area was decreased with particle size in order to always afford 2-3 pixels for each individual particle. Under this limitation, the resolution of the camera (2016×2016 pixels) was sufficient to cover the entire 0.3 m bed width for the 350 and 500 µm particle sizes, but only 2/3 of the bed width for the 250 µm particles. The bed also expanded to more than 0.3 m for most of the cases studied requiring a vertical displacement of the camera to cover the whole bed height. Image pairs were collected at a frequency of 4 Hz with a time delay of 2-4 ms between the two images in each pair. The commercial software package Davis was used for post-processing the images and for determining the particle velocity fields.

The sensitivity of the average particle velocity to the number of images was investigated for a base case by averaging over 500, 800, 1200, 1500 and 2200 images. The average value of each group of images was measured and analysed according to the procedure used by de Jong et al. [20] and 800 images was found to be sufficient for calculating accurate flow statistics.

5 Simulations

Simulations were carried out on a 2D planar geometry using the standard TFM with the set of closure laws most widely used in the literature. No new modelling options were investigated since the aim of this work is simply to establish a baseline comparison from which further research can follow.

5.1 Model equations

Conservation equations are solved for each of the two phases present in the simulation. The continuity equations for the gas and solids phases phase are given below:

$$\frac{\partial}{\partial t}\left(\alpha_g \rho_g\right)+\nabla\cdot\left(\alpha_g \rho_g \vec{\upsilon}_g\right)=0 \qquad \text{Equation 1}$$

$$\frac{\partial}{\partial t}\left(\alpha_s \rho_s\right)+\nabla\cdot\left(\alpha_s \rho_s \vec{\upsilon}_s\right)=0 \qquad \text{Equation 2}$$

Momentum conservation for the gas phase is written as

$$\frac{\partial}{\partial t}\left(\alpha_g \rho_g \vec{\upsilon}_g\right)+\nabla\cdot\left(\alpha_g \rho_g \vec{\upsilon}_g \vec{\upsilon}_g\right)=-\alpha_g \nabla p+\nabla\cdot\bar{\bar{\tau}}_g+\alpha_g \rho_g \vec{g}+K_{sg}\left(\vec{\upsilon}_s-\vec{\upsilon}_g\right) \qquad \text{Equation 3}$$

And for the solids as

$$\frac{\partial}{\partial t}\left(\alpha_s \rho_s \vec{\upsilon}_s\right)+\nabla\cdot\left(\alpha_s \rho_s \vec{\upsilon}_s \vec{\upsilon}_s\right)=-\alpha_s \nabla p-\nabla p_s+\nabla\cdot\bar{\bar{\tau}}_s+\alpha_s \rho_s \vec{g}+K_{gs}\left(\vec{\upsilon}_g-\vec{\upsilon}_s\right) \qquad \text{Equation 4}$$

The inter-phase momentum exchange coefficient $\left(K_{gs}=K_{sg}\right)$ was modelled according to the formulation of Syamlal and O'Brian [21].

Solids phase stresses were determined according to the KTGF analogy where the random particle motion is likened to the thermal motion of molecules in a gas using the concept of granular temperature. The conservation equation for granular temperature is given below:

$$\frac{3}{2}\left[\frac{\partial}{\partial t}\left(\alpha_s \rho_s \Theta_s\right)+\nabla\cdot\left(\alpha_s \rho_s \vec{\upsilon}_s \Theta_s\right)\right]=\left(-p_s \bar{\bar{I}}+\bar{\bar{\tau}}_s\right):\nabla \vec{\upsilon}_s+\nabla\cdot\left(k_{\Theta_s}\nabla\Theta_s\right)-\gamma_{\Theta_s}+\phi_{gs} \qquad \text{Equation 5}$$

This partial differential equation was simplified to an algebraic equation by neglecting the convection and diffusion terms – an often used assumption in dense, slow moving fluidized beds where the local generation and dissipation of granular temperature far outweigh the transport by convection and diffusion [22]. The two final terms in Equation 5 are the collisional dissipation of energy [1] and the interphase exchange between the particle fluctuations and the gas phase [23].

Solids stresses are calculated according to shear and bulk [1] viscosities due to particle momentum exchange through translation and collision. The shear viscosity consists of three parts: collisional [21, 23], kinetic [21] and frictional [24].

Granular temperature as well as the radial distribution function (measure of the average distance between particles) is used to determine the solids pressure (p_s in Equation 4). The solids pressure formulation by Lun et al. [1] was complemented by the radial distribution function of Ogawa and Oshima [25].

5.2 Boundary conditions

A simple no-slip wall boundary condition was set for the gas phase. The Johnson and Jackson [26] boundary condition was used for the granular phase with a specularity coefficient of 0.5.

$$\vec{\tau}_s=-\frac{\pi}{6}\sqrt{3}\varsigma\frac{\alpha_s}{\alpha_{s,\max}}\rho_s g_{0,ss}\sqrt{\Theta_s}\vec{U}_{s,\|} \qquad \text{Equation 6}$$

The inlet condition was specified as a velocity inlet according to the specific simulation run in question and the outlet was designated as a pressure outlet at atmospheric pressure.

5.3 Flow solver and solver settings

The commercial software package, FLUENT 13.0 was used as the flow solver. The phase coupled SIMPLE scheme [27] was used for pressure-velocity coupling and the higher order QUICK scheme [28] for the spatial discretization of all remaining equations. First order implicit temporal discretization was used. It has been shown that 2nd order time discretization is necessary for accurate solution of fast-moving riser flows with the TFM [16], but this is not the case for dense bubbling beds where the vast majority of the bed moves relatively slowly.

5.4 Geometry and meshing

The pseudo-2D experimental unit was approximated as a 2D plane for simulation purposes. Like the experimental unit, this plane was 0.3 m in width and 1.5 m in height. Meshing was done using a simple structured grid of completely square cells. Many cell sizes were evaluated in a grid independence study (section 7.1) based on refinement of a grid of 1 cm cells.

Refinement was done by hanging node adaption only in the lower part of the domain where the bed material resides. This method of grid refinement prevented excessively fine cells in the freeboard region where accurate resolution of the flow field is not important.

5.5 Initial conditions

The solution was initialized with zero velocity and no solids, after which solids were patched in at a volume fraction of 0.6 to the initial static bed height used in the specific experiment. The solution was run for 5 seconds in order to attain a quasi-steady flow condition. This solution was then used as the initial condition for time-averaging.

5.6 Simulation summary

A summary of the physical properties and simulation parameters are given in Table 1.

Table 2: Physical properties and simulation parameters

Gas density	1.225 kg/m^3
Gas viscosity	1.789x10^{-5} kg/m·s
Particle density	2500 kg/m^3
Particle sizes	90, 150, 250, 350 & 500 µm
Bed dimensions	0.3 x 1.5 m^2
Particle-particle restitution	0.9
Specularity coefficient	0.5
Angle of internal friction	30°
Friction packing limit	0.55
Maximum packaging limit	0.63

6 Data collection and processing

6.1 Performance measures

The primary performance measure extracted from each run is the bed expansion ratio. This measure was defined as the average height of the 10% time averaged volume fraction threshold as calculated by the CFD simulation divided by the initial static bed height.

The expanded bed height could easily be directly extracted from the CFD simulations, but more processing was required to find the equivalent measure from the experiments by means of image analysis. This was done by averaging the volume fraction field produced by 200 experimental images and finding the height of the correct grey threshold. The appropriate threshold was determined by averaging an equivalent number of CFD images and determining the threshold at which the simulation calculates the 10% volume fraction as illustrated in Figure 2.

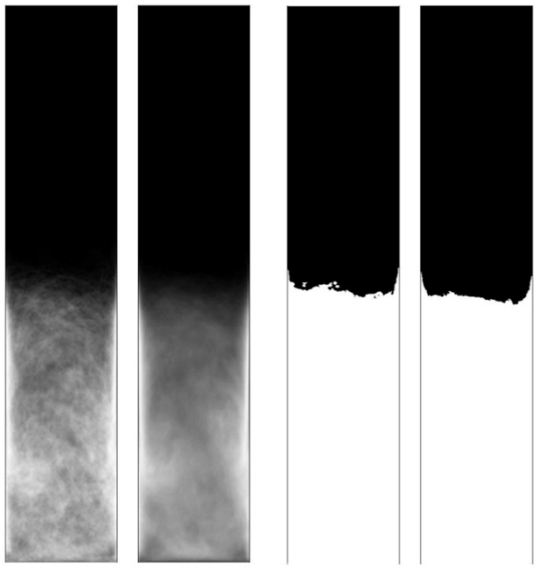

Figure 2: Simulated volume fraction plots as created by averaging images (left) and by numerical time averaging (second to left). The 10% volume fraction threshold was determined numerically (far right) and reproduced as a greyscale threshold (second to right).

As shown in Figure 3, the same greyscale threshold was subsequently used on averaged experimental images in order to approximate the 10% volume fraction threshold.

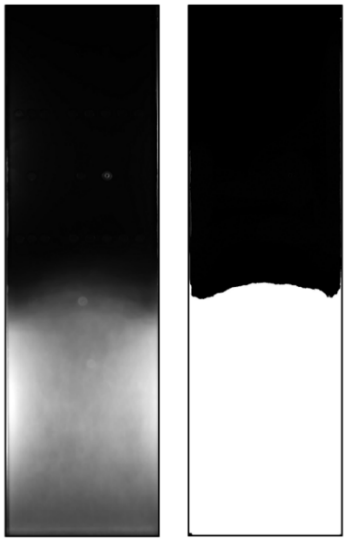

Figure 3: An example of the experimental volume fraction plot averaged from 200 images (left) as well as the approximated 10% volume fraction threshold (right).

As will be seen later, this method delivers reliable results that contain statistically very small measurement errors.

6.2 Data analysis

The results and subsequent analysis was based on a three factor central composite design [29]. This is a form of experimental design where the response of any specific dependent variable (e.g. the bed expansion ratio discussed in the previous section) to changes in various independent variables can be easily assessed, accurately quantified and visualized. The three independent variables, henceforth called factors, considered in the design were specified over five levels as follows:

- Gas flow rate (U). This factor was evaluated at gas injection velocities of 0.264, 0.4, 0.6, 0.8 and 0.936 m/s. These velocities produced fluidization falling in the bubbling fluidization regime for all the runs in the central composite design.
- Static bed height (H). The initial packed bed height was evaluated at five levels: 0.132, 0.2, 0.3, 0.4 and 0.468 m. These measures ensured significant variations in the expanded bed height, but kept the bed material from over-expanding out of the experimental unit.
- Particle diameter (d). Five constant particle sizes were used: 90, 150, 250, 350 and 500 µm. Ideally, the particle sizes chosen would be 82, 150, 250, 350 and 418 µm to maintain rotatability of the design. Rotatability is the characteristic that all experimental points are located at the same normalized distance from the centrepoint of the design (U = 0.6 m/s, H = 0.3 m and d = 250 µm) and is a desirable property for optimization studies. In this case, however, an optimal point is not expected within the parameter space, but rather a steady increase or decrease. Accuracy will therefore not be significantly affected by the partial rotatability of this design.

The central composite design was run for the experiments and the simulations, requiring 16 runs in each case (Table 2). This facilitated a direct and easily quantifiable comparison between experimental and simulation results. This paper will focus on quantifying the differences between these results.

Table 3: Case specification for the 16 runs in the central composite design completed both for the experiments and the simulations together with the simulated and experimental bed expansion ratios.

Case number	Fluidization velocity (m/s)	Static bed height (m)	Particle size (µm)	Experimental bed expansion ratio	Simulated bed expansion ratio
1	0,4	0,2	150	1,95	1,92
2	0,4	0,2	350	1,61	1,40
3	0,4	0,4	150	1,55	1,81
4	0,4	0,4	350	1,37	1,34
5	0,8	0,2	150	2,78	2,52
6	0,8	0,2	350	2,41	1,98
7	0,8	0,4	150	2,05	2,40
8	0,8	0,4	350	1,71	1,88
9	0,264	0,3	250	1,38	1,32
10	0,936	0,3	250	2,32	2,29
11	0,6	0,132	250	2,48	2,01
12	0,6	0,468	250	1,69	1,77
13	0,6	0,3	90	2,76	2,53
14	0,6	0,3	500	1,73	1,46
15 (C)	0,6	0,3	250	1,86	1,87
16 (C)	0,6	0,3	250	1,84	1,87

The differences between simulation and experiment were quantified and visualised as the percentage by which the simulations differed from the experiments for each case. This provided very informative trends on how the difference between simulation and experiment changed with changes in the three factors involved.

Results will primarily be displayed in two ways: an analysis of variance (ANOVA) and response surfaces of dependent variables to changes in various factors. The ANOVA will be used to identify the most significant factors in the design (i.e. factors where the simulations responded differently from the experiments as the factor is changed). In this manner, the generic applicability of the CFD was strictly evaluated.

The significance of factors will be defined by the p-value which is an indication of the probability of the observed effect to arise from pure random chance. If this value becomes small $\left(p < 0.05\right)$, the effect is said to be significant because the probability of it occurring by random chance is sufficiently small. A value of $p < 0.01$ is generally regarded as highly significant. The p-value is calculated from the F-test which weighs the amount of explained variance in the design against the amount of unexplained variance (experimental error, rounding error, averaging error, data not fitting the second order model etc.). This ratio can then be evaluated as a p-value to decide whether any observed variance is caused by a significant effect or whether it is simply random.

The relative variance explained by each factor will also be given as the percentage of the total sum of squares (SS). The total sum of squares for a specific dependent variable is the sum of all the squared differences between all the experimental points and the mean. A larger total sum of squares implies that experimental observations are scattered wide around the mean and there is a lot of variance in the design. This measure will give an indication of the importance of significant effects relative to each other.

Once the significant effects are identified in this way, the difference between simulation and experiment will be plotted on a response surface as a function of these highly significant factors in order to gain an understanding of the nature of any significant difference.

In case more details are sought, the interested reader is referred to the aforementioned reference [29] for a more detailed theoretical description of a central composite design.

7 Results and discussion

Results will be presented and discussed in four sections: an extensive grid independence study, results from the central composite design, some visual comparisons between simulation and experiment, and finally some more detailed velocity profile comparisons.

7.1 Grid independence study

It is well known that the grid independence behaviour of fluidized bed simulations is strongly dependent on particle size. Since a wide range of particles sizes is considered in this study, it is important that the correct cell size is used for each run in order to ensure accurate results while simultaneously maintaining reasonable simulation times.

Each of the 15 unique runs in the design (the centre point of the design is done twice) were therefore run on grid spacings ranging from a maximum of 1 cm to the small grid size necessary for grid independence. Two performance measures were extracted to indicate grid independence: the expanded bed height (Table 3) and the integral of the RMS volume fraction over the entire bed (Table 4).

Table 4: The expanded bed height for different cell sizes.

Case number	Particle size (µm)	10 mm	5 mm	2.5 mm	1.25 mm	0.625 mm	0.313 mm
13	90		0,957	0,839	0,798	0,760	0,730
1	150	0,476	0,420	0,406	0,390	0,384	
5	150	0,569	0,551	0,529	0,518	0,503	
3	150	0,791	0,745	0,724	0,710	0,708	
7	150	1,040	1,005	0,960	0,933	0,930	
11	250	0,272	0,271	0,265	0,261		
9	250	0,398	0,397	0,395	0,397		
10	250	0,715	0,717	0,705	0,701		
15 (C)	250	0,579	0,570	0,561	0,561		
12	250	0,858	0,847	0,828	0,838		
2	350	0,276	0,280	0,281	0,283		
6	350	0,396	0,400	0,395	0,396		
4	350	0,532	0,533	0,536	0,537		
8	350	0,752	0,749	0,750	0,736		
14	500	0,429	0,433	0,436	0,438		

Table 5: The integral of the RMS volume fraction for different cell sizes.

Case number	Particle size (µm)	10 mm	5 mm	2.5 mm	1.25 mm	0.625 mm	0.313 mm
13	90		0,0401	0,0540	0,0563	0,0588	0,0592
1	150	0,0226	0,0269	0,0289	0,0300	0,0311	
5	150	0,0298	0,0351	0,0383	0,0402	0,0409	
3	150	0,0418	0,0489	0,0520	0,0541	0,0568	
7	150	0,0519	0,0642	0,0685	0,0719	0,0741	
11	250	0,0158	0,0180	0,0192	0,0201		
9	250	0,0194	0,0231	0,0247	0,0263		
10	250	0,0435	0,0469	0,0495	0,0502		
15 (C)	250	0,0350	0,0376	0,0394	0,0420		
12	250	0,0526	0,0563	0,0583	0,0624		
2	350	0,0145	0,0170	0,0184	0,0196		
6	350	0,0251	0,0269	0,0288	0,0301		
4	350	0,0284	0,0317	0,0341	0,0355		
8	350	0,0466	0,0488	0,0515	0,0538		
14	500	0,0240	0,0264	0,0283	0,0305		

In order to better visualize these results, the percentage change in each performance measure with a halving of the cell size was plotted for each case in Figure 4 and Figure 5.

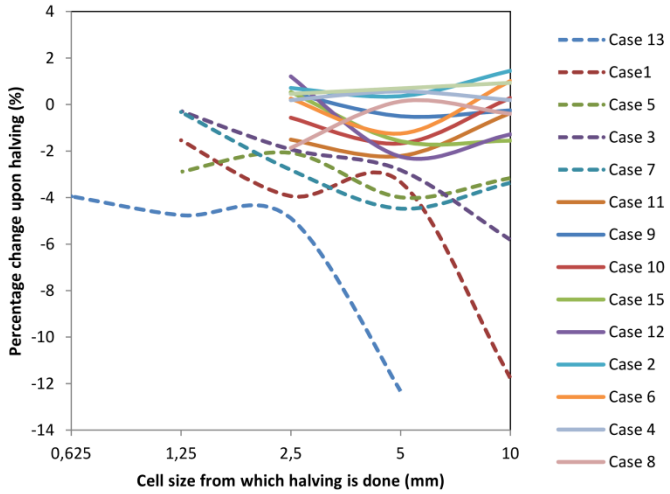

Figure 4: Percentage change in the expanded bed height with a halving of the cell size. The cases run with small particles (90 µm and 150 µm) are shown in dashed lines. Individual cases can only be distinguished in the colour version of this figure in the online version of this paper.

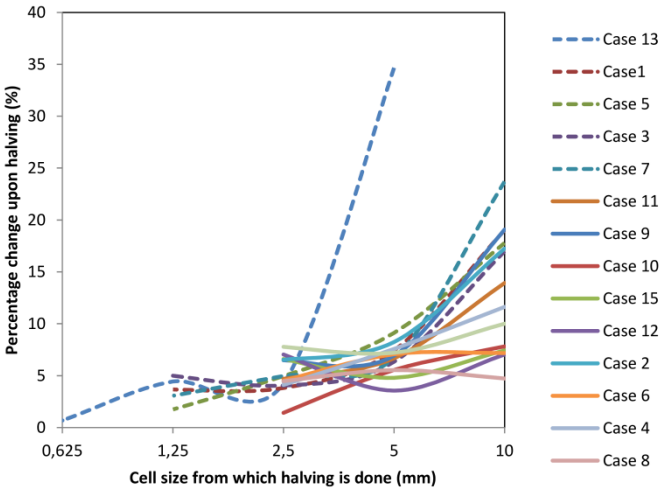

Figure 5: Percentage change in the integral of the RMS volume fraction with a halving in the cell size. The cases run with small particles (90 µm and 150 µm) are shown in dashed lines. Individual cases can only be distinguished in the colour version of this figure in the online version of this paper.

Inspection of Figure 4 and Figure 5 shows that the grid independence behaviour of the two chosen performance measures is distinctly different. The bed height performance measure showed a strong dependence on particle size. All cases with particle sizes of 250 µm and above gave sufficiently grid independent results (judged as a 2% or smaller change in the solution as the cell size is halved) essentially at all the grid sizes. Since bed expansion ratio is the primary performance measure in this study and sufficient grid independence with regards to this parameter is achieved on affordable grids, expensive finer grid simulations were not completed for these cases. The 150 µm and 90 µm cases, on the other hand, showed greater grid dependence effects and more expensive, fine grid simulations therefore had to be completed. For the 90 µm case, grid independence could not be achieved even on a very expensive simulation using 0.313 mm cells (3.5 particle diameters).

Another interesting trend from Figure 4 is that only smaller particle sizes exhibit the expected reduction of expanded bed height with grid refinement (the percentage change upon halving is negative). This is a natural result of better resolution of mesoscale particle structures which slip much more readily past

the fluidizing gas, causing a more compact bed. For larger particle sizes, however, this trend seems to reverse with expanded bed heights actually becoming larger with increased grid refinement (the percentage change upon halving becomes positive). The changes from one grid to the next are very small, however, and therefore do not merit further attention.

In the case of the integral of the RMS volume fraction, the results were much less dependent on particle size. This variable was also much more sensitive to changes in the grid spacing and sufficiently grid independent behaviour could not be attained for most cases. This performance measure was not used to compare to experimental results, however, and is therefore of lesser importance for this particular study, but this potential source of unexplained variance should be kept in mind for the remainder of this study and further explored in future work.

In general, the grid independence behaviour of these two performance measures can be explained by acknowledging that increases in the RMS volume fraction as the grid is refined indicates increases in the degree to which phase segregation is resolved, while decreases in the expanded bed height with grid refinement is the effect of this increased phase segregation. As mentioned before, well resolved clusters of particles slip much more readily relative to the fluidizing gas and better resolved particle clusters should therefore result in a more compact bed. This effect is much more prominent for small particles since the individual particle drag on these particles is much larger. For this reason, increases in the resolution of the phase segregation with grid refinement will have a larger impact on the expanded bed height of beds with smaller particles than on beds with larger particles even though the degree of phase resolution itself seems to be largely independent of particle size.

For the remainder of this study, the results from the 2.5 mm grid will be used for the particle sizes of 250, 350 and 500 µm, results from the 0.625 mm grid will be used for the 150 µm particles and results from the 0.313 mm grid for the 90 µm particles.

7.2 Results from the central composite design

Firstly, the second order model was fit through the experimental and the simulation data given in Table 2 in order to assess whether the data provided meaningful trends. The model has the following form:

$$X = C_1U + C_2U^2 + C_3H + C_4H^2 + C_5d + C_6d^2 + C_7UH + C_8Ud + C_9Hd \qquad \text{Equation 7}$$

Here, X is the specific dependent variable (in this case the bed expansion ratio), C_1 through C_9 are constants producing the best fit to the data and U, H and d are the factors of fluidization velocity, static bed height and particle diameter.

Upon analysis of the data it was found that it is best to omit the 90 µm case from the study since a significant amount of uncertainty was linked to this case both from an experimental and simulation point of view. For the experiments, the expanded bed height was difficult to measure since some fines were continuously fluidized into the freeboard, making the expanded bed seem to be taller than it actually was (see Figure 9). For the simulations, sufficiently grid independent results could not be attained. Data could be extracted from all of the remaining cases with a large degree of accuracy, however, and a very good model fit to the data was attained according to Equation 7.

The ANOVA results for the two sets of data are given in Table 5.

Table 6: ANOVA table summarizing the response of bed expansion ratio returned by the experiments and the simulations to changes in the three factors investigated. Significant factors are shown in bold, while highly significant factors are shown in bold italics. The factors are denoted by U (fluidization velocity), H (static bed height), and d (particle diameter). Different effects are indicated by L (linear), Q (quadratic) and by (interaction).

Effect	Experiments		Simulation	
	SS (%)	p-value	SS (%)	p-value
U(L)	***49,90***	***0,0000***	***60,72***	***0,0000***
U(Q)	0,01	0,7712	**0,19**	**0,0296**
H(L)	***35,06***	***0,0000***	***3,05***	***0,0001***
H(Q)	***2,16***	***0,0076***	0,04	0,2303
d(L)	***7,54***	***0,0005***	***33,62***	***0,0000***
d(Q)	**1,09**	**0,0281**	***1,95***	***0,0002***
U(L) by H(L)	***3,30***	***0,0031***	0,05	0,1695
U(L) by d(L)	0,20	0,2437	0,09	0,0854
H(L) by d(L)	0,15	0,3007	**0,19**	**0,0291**
Error	0,58		0,10	
Total	100,00		100,00	

From the very small amount of error variance present in Table 5, it is clear that a near perfect fit is achieved for both sets of data, confirming that both simulations and experiments were highly repeatable. The data shows that linear effects dominate over quadratic and interaction effects, indicating that simple linear increases and decreases of the bed expansion ratio with changes in the three factors investigated. It is also clear that, while the experimental and simulation results respond very similarly to changes in the fluidization velocity, their response to changes in the static bed height and particle size differs significantly. In the experiments, the bed expansion ratio seems to be much more dependent on the static bed height than on the particle size, while the simulations predict exactly the opposite.

The nature of this difference can be further investigated by completing the central composite design for the percentage deviation of the simulation result from the experimental result $\left(\left(\left(H/H_0\right)_{sim}-\left(H/H_0\right)_{\exp}\right)\Big/\left(H/H_0\right)_{\exp}\times 100\%\right)$ in each data point. The ANOVA results of this analysis are given in Table 6.

Table 7: ANOVA table summarizing the response of the deviation of simulation predictions from experimental observations of the bed expansion ratio to changes in the three factors investigated. Significant factors are shown in bold, while highly significant factors are shown in bold italics. The factors are denoted by U (fluidization velocity), H (static bed height), and d (particle diameter). Different effects are indicated by L (linear), Q (quadratic) and by (interaction).

Effect	SS (%)	p-value
U(L)	0,15	0,7200
U(Q)	0,44	0,5442
H(L)	***60,77***	***0,0006***
H(Q)	3,11	0,1449
d(L)	***24,37***	***0,0047***
d(Q)	0,07	0,8108
U(L) by H(L)	4,45	0,0937
U(L) by d(L)	1,42	0,2956
H(L) by d(L)	0,01	0,9218
Error	5,22	
Total	100,00	

As expected, Table 6 indicates that the simulation differs significantly from experiments in its response to changes in the static bed height and the particle size, while no difference is observed in the response to changes in the fluidization velocity. The nature of these deviations is shown in Figure 6.

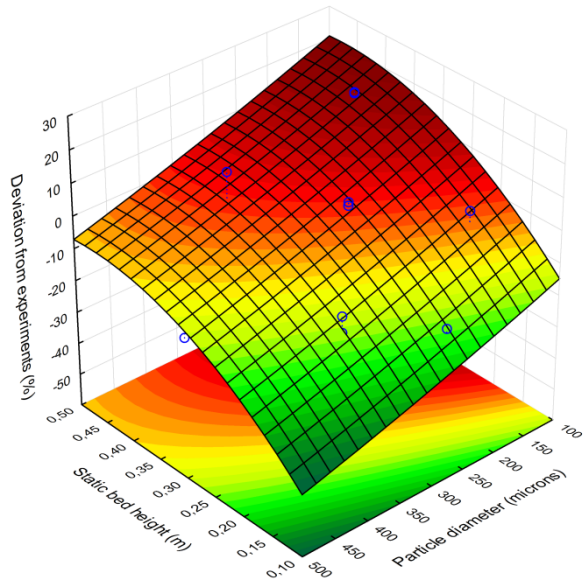

Figure 6: Response surface of the changes in the percentage deviation between simulation and experiment to changes in the static bed height and the particle size.

Simulation predictions of the bed expansion differ from experiments by between -40% at low static bed heights and large particle sizes and 22% at large static bed heights and small particle sizes. In other words, the simulations under-predicted the bed expansion for low static bed heights and large particles and over-predicted results for large static bed heights and small particles. These deviations will be further discussed in subsequent sections.

7.3 Qualitative visual comparisons

An immediate idea of the accuracy of the numerical solution can be gained by direct comparisons of the instantaneous volume fraction distributions. These comparisons are given in Figure 7, Figure 8 and Figure 9 to illustrate the response of the experiments and the simulations to changes in the three factors investigated.

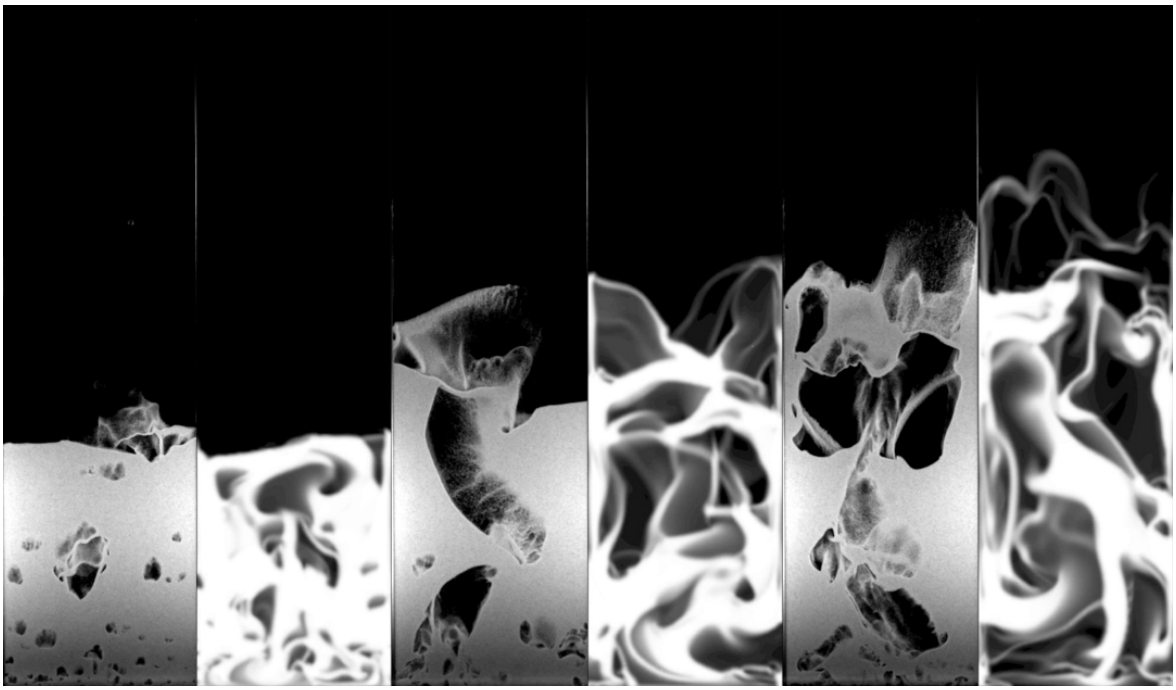

Figure 7: Visual comparison of the bed dynamics of the experiments and the simulations as the fluidization velocity is increased. The three pairs of images from left to right are from cases 9, 15 and 10.

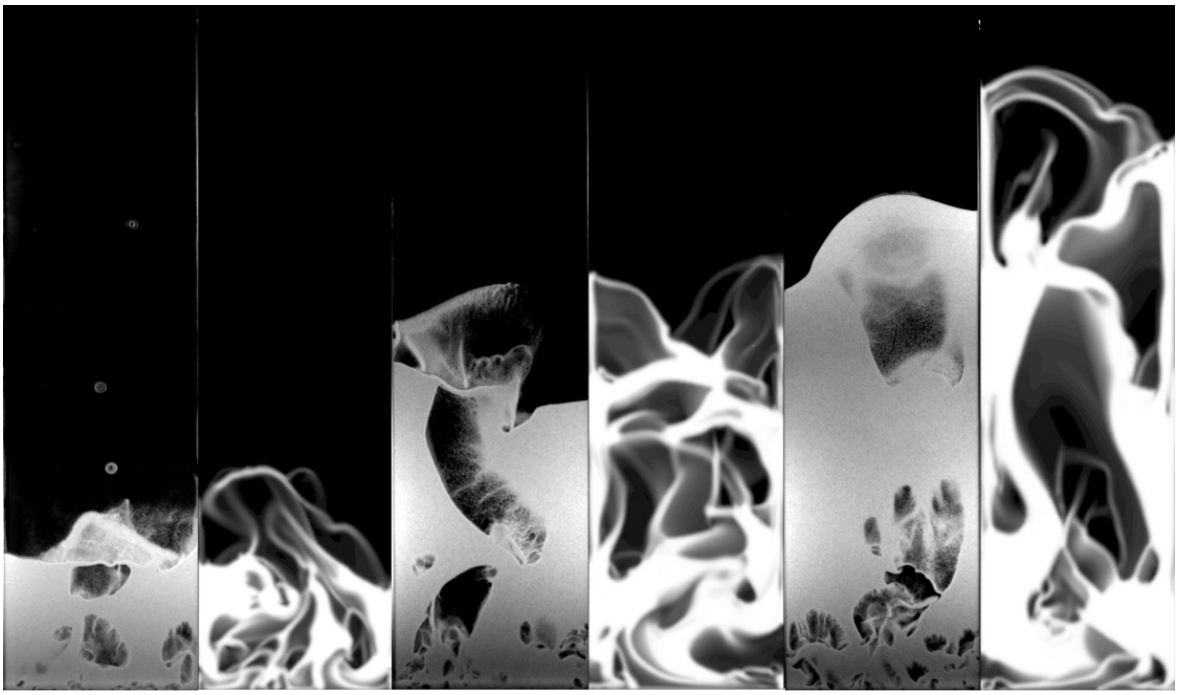

Figure 8: Visual comparison of the bed dynamics of the experiments and the simulations as the static bed height is increased. The three pairs of images from left to right are from cases 11, 15 and 12.

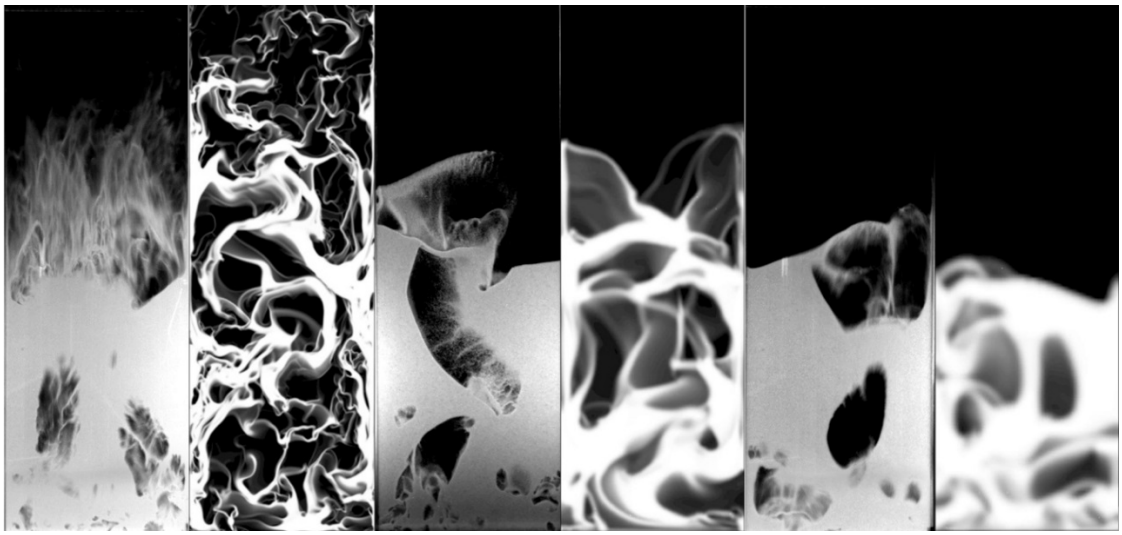

Figure 9: Visual comparison of the bed dynamics of the experiments and the simulations as the particle size is increased. The three pairs of images from left to right are from cases 13, 15 and 14.

The following generic differences between simulation and experiment can be identified:

- The simulations generally predict larger and more distorted bubbles.
- The experiments show more coherent flow structures, especially close to the distributor.
- It appears as if the simulations contain less emulsion phase than the experiments

Despite these differences, Figure 7, Figure 8 and Figure 9 seem to suggest adequate qualitative model behaviour, at least when it comes to predicting the bed height. The systematic simulation errors observed in Figure 6 can be identified even from these instantaneous plots, however. The under-predictions of bed expansion ratio at low static bed heights seem to be due to the inadequate resolution of small, slow rising bubbles, while the over-prediction at high static bed heights seem to be due to the formation of large slug-like bubbles. For the particle size, the difference between simulation and experiment when 90 µm particles are used is especially pronounced. Simulations show a significant over-prediction of the void fraction as well as bubble dynamics which are distinctly different from experimental observations. It is possible that this is primarily due to the negligence of inter-particle forces which could become significant for Geldart A powders. The prediction of bubble dynamics seems to improve as the particle size is increased, but leads to under-predictions of the bed height at large particle sizes. These systematic differences will be investigated in greater detail in future works.

When reactive simulations are run in future works, the deviation between simulation and experiment is likely to worsen considerably, primarily because the degree of conversion is strongly dependent on the quality of gas-solid contact which, in turn, is strongly dependent on the resolution of phase segregation. The significant errors in simulation prediction of bubble dynamics, particularly at high fluidization velocities, high static bed heights and small particle sizes are likely to lead to considerable errors in the prediction of reactor performance (degree of conversion achieved) when reactive simulations are run. In addition, the incomplete phase segregation grid independence behaviour (Figure 5) is also likely to have a much larger impact on reactant conversion than it has on hydrodynamic measures like the bed expansion ratio. Future work will be focussed on this topic.

The impression that the simulations contain less emulsion phase than the experiments can be due to three factors. Firstly, the simulations showed the emulsion phase to almost universally be very close to

the maximum packing limit, while this is not always the case in experiments [30]. Hence, it could be that the emulsion phase in experiments is less concentrated and therefore spread over a larger area. Secondly, the inherent 3D nature of the experiments will reduce the observed area of bubbles if any degree of non-uniformity in the solids volume fraction across the thickness of the unit occurs. And finally, experimental particle volume fractions of less than 0.3 might already completely obscure the dark back plate, giving the false impression of a fully compacted emulsion phase. It is expected that the latter two points are primarily responsible for the observed effect.

7.4 PIV velocity profiles

Finally, some more detailed comparisons between simulations and experiments will be made by means of comparing lateral velocity profiles. It would have been ideal if velocity measurements could be carried out for all cases listed in Table 2, but this was not possible because the PIV technique required larger particles in order to cover a meaningful area of the experimental unit. For this reason, seven new experimental cases were completed.

Table 8: Case specifications for the PIV study

Case	Fluidization velocity (m/s)	Static bed height (m)	Particle size (µm)
1	0,6	0,3	500
2	0,4	0,3	500
3	0,8	0,3	500
4	0,6	0,2	500
5	0,6	0,4	500
6	0,6	0,3	350
7	0,6	0,3	250

As Table 7 illustrates, Case 1 serves as a common point from which all three variables are varied. The majority of cases were completed using 500 µm particles to allow for better PIV measurements.

In order to facilitate a meaningful comparison of simulation to experiment for all seven cases, only one cross-stream y-velocity profile, that which resides at the initial static bed height, will be plotted for each case. The experimental data is given in Figure 10 and the simulated profiles in Figure 11. For the simulations, only velocity values in regions with a solids volume fraction of 0.12 and above were incorporated in the averaging – a procedure similar to that used in the experiments.

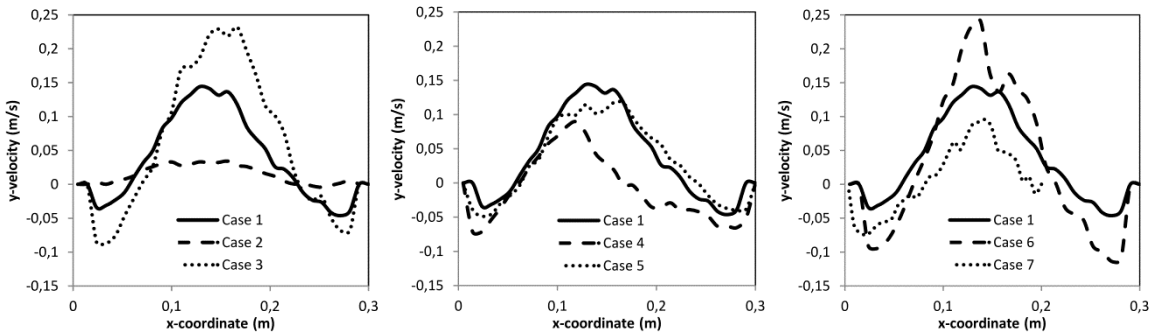

Figure 10: Experimental cross-stream y-velocity profiles at the height of the static bed.

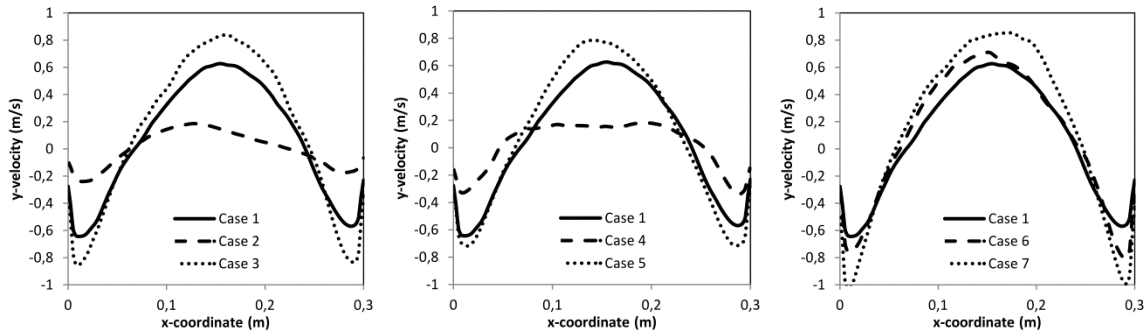

Figure 11: Simulated cross-stream y-velocity profiles at the height of the static bed.

The first observation from the data is that the simulated velocities are much higher than the experimental ones. For case 1, the velocities seem to be about 4 times higher. This is certainly a very large discrepancy and implies that the 2D assumption used in this study is greatly in error.

The only factor that can cause such a large discrepancy is the frictional stresses on the large front and back walls of the pseudo-2D experimental unit. This factor is not accounted for in 2D simulations which, in essence, assume free-slip boundary conditions at the front and back walls of the pseudo-2D reactor.

Qualitatively, a similar response to changes in the three different factors is obtained between simulations and experiment, but the large quantitative difference makes it hard to draw any clear conclusions in this regard.

In order to further investigate this very large discrepancy, two 3D simulations were run for Case 1 in Table 7: one with free-slip front and back walls and one where the specularity coefficient in Equation 6 was set to 0.5. The specularity coefficient at the side walls was kept at 0.5 for both simulations to be consistent with the 2D simulations. Similarly to the 2D simulations, 2.5 mm cells were used. A 1.25 mm cell thickness was implemented in the third dimension, creating 12 cells along the thickness of the reactor in order to achieve adequate resolution of any 3D effects.

Solids velocity results from these two new cases are compared directly to the 2D case and the experiments in Figure 12.

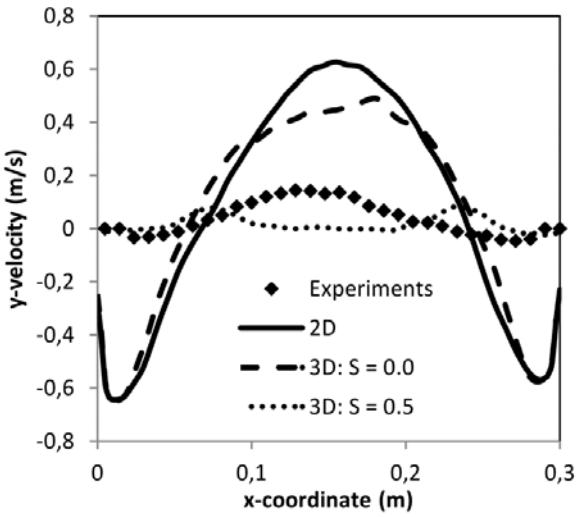

Figure 12: Time averaged y-velocity profiles for Case 1 at a height of 0.3 m. Experiments are compared to simulation results from a 2D geometry as well as two 3D simulations with specularity coefficients of 0 and 0.5 on the large front and back walls.

It is clear that the effect of friction on the front and back walls of the reactor is very large. Figure 12 shows that the 3D simulation with no friction on the front and back walls gives very similar results to that of the 2D simulation, implying that the inclusion of the third dimension made no significant difference. When friction was included on the front and back walls, however, the solids velocities were drastically reduced to the level of those measured in the experiments.

In fact, it can be speculated that the friction incorporated in this simulation was too strong, not allowing the bubbles to travel laterally, but only rising in two streams about one quarter of a width in from both side walls (Figure 13). This can also be seen from Figure 12 where the experimental velocities peak in the centre and the simulation shows two peaks on both sides of the centre. Further investigations into the effect of the specularity coefficient are postponed for future studies though.

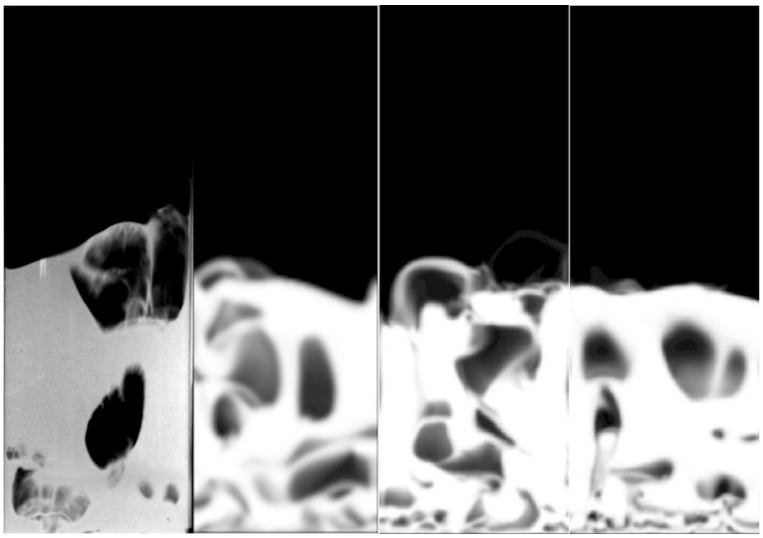

Figure 13: Instantaneous volume fraction fields from the cases plotted in Figure 12. From left to right: experiment, 2D simulation, 3D simulation without friction at the front and back walls, and 3D simulation with friction on all walls.

It is interesting to note how little influence this very large solids velocity discrepancy has on the overall bed behaviour. From Figure 13 it appears that the expanded bed heights returned by the three simulations are virtually identical. Qualitative bubble characteristics also do not show very large differences, except for the 3D simulations resolving smaller bubbles close to the inlet.

The very small effect of solids velocity on the bed height is somewhat surprising. It would be expected that the simulation with large friction at the walls would severely obstruct the flow of gas through the bed, thereby slowing down the bubbles and leading to a more expanded bed. When studying animations of these simulations, however, it can be seen that the free-flowing solids (no wall friction) behave very liquid-like and regularly create strong back-mixing zones that interfere with rising bubbles, thereby trapping more gas inside the bed. The restricted solids (large wall friction) does slow down the bubbles, but most bubbles rise straight upwards and are not influenced by any backflows. The 3D simulation with wall friction reported in Figure 12 and Figure 13 also established two channels of continuous bubble motion as described earlier, thereby allowing bubbles to rise very efficiently through the bed without causing much bed expansion. Due to this effect, the gas-holdup of these two very different flow scenarios is quite similar.

If it is assumed that the discrepancies in bed expansion ratio shown in Figure 6 are primarily due to this very large error in the solids velocity predictions, it can be preliminarily concluded that the solids velocity

has a small, but rather complex influence on the gas holdup in the bed. In some circumstances, this error seems to over-predict the bed expansion (large static bed heights and small particle sizes), while under-predictions are observed in other cases (small static bed heights and large particle sizes). Further study will be directed towards understanding these effects.

The differences in bubble dynamics displayed in Figure 7, Figure 8 and Figure 9 can also be related to the large differences in solids velocities observed in Figure 10 and Figure 11. It was remarked that the simulated bubbles are more elongated and distorted. This effect is reasoned to be due to the much higher and more chaotic velocities prevalent in 2D simulations not accounting for the large friction at the front and back walls.

In general, it appears that even very large errors in the prediction of the solids velocity still leads to reasonable macroscopic bed behaviour (average gas holdup and bubble size) in many cases, implying that a large margin for error exists in purely hydrodynamic bubbling fluidized bed simulations. Further studies on this topic should include reaction kinetics in order to quantify the effect of this error on the prediction of overall reactor performance, a performance measure which is likely to be significantly more sensitive to error as observed in [15].

8 Conclusions

Experiments were carried out in a pseudo-2D bubbling fluidized bed over a wide range of different fluidization velocities, bed loadings and particle sizes. The bed expansion ratio was determined for each case and compared to results from simulations carried out with the standard 2D TFM closed by the KTGF. Systematic differences were observed between simulations and experiments depending on the setting of the flow variables.

Bed expansion ratios derived from experiments and simulations responded similarly to changes in the fluidization velocity, but distinct differences in the response to changes in bed loading and particle size were observed. In general, simulations under-predicted the bed expansion ratio at low bed loadings and large particle sizes and over-predicted the bed expansion ratio at high bed loadings and small particle sizes. The systematic difference between bed expansion ratios returned by simulations and experiments varied smoothly over the parameter space.

Qualitative comparisons between instantaneous volume fraction profiles photographed in the experiments and calculated in the simulations showed that simulations generally predicted larger and more distorted bubbles, with the difference becoming increasingly pronounced towards smaller particle sizes. The comparisons also showed that simulations did not adequately capture small bubbles formed close to the gas distributor.

A very large factor of four difference between experimental and simulated particle velocities was identified as the largest quantitative difference between simulations and experiments. The large over-prediction of particle velocity observed in the experiments was due to the friction on the large front and back walls not being accounted for in the 2D simulations. 3D simulations were carried out to confirm this notion and further work was recommended on this topic.

9 Acknowledgements

The authors would like to acknowledge the funding received from the Research Council of Norway which enabled the completion of this work.

10 References

1. Lun, C.K.K., et al., *Kinetic Theories for Granular Flow: Inelastic Particles in Couette Flow and Slightly Inelastic Particles in a General Flow Field.* Journal of Fluid Mechanics, 1984. **140**: p. 223-256.
2. Jenkins, J.T. and S.B. Savage, *Theory for the rapid flow of identical, smooth, nearly elastic, spherical particles.* Journal of Fluid Mechanics, 1983. **130**: p. 187-202.
3. Sun, J., et al., *CFD simulation and experiments of dynamic parameters in gas–solid fluidized bed.* Chemical Engineering Science, 2011. **66**(21): p. 4972-4982.
4. Hulme, I., et al., *CFD Modeling and Validation of Bubble Properties for a Bubbling Fluidized Bed.* Industrial & Engineering Chemistry Research, 2005. **44**(12): p. 4254-4266.
5. Johansson, K., B.G.M. van Wachem, and A.E. Almstedt, *Experimental validation of CFD models for fluidized beds: Influence of particle stress models, gas phase compressibility and air inflow models.* Chemical Engineering Science, 2006. **61**(5): p. 1705-1717.
6. Patil, D.J., M. van Sint Annaland, and J.A.M. Kuipers, *Critical comparison of hydrodynamic models for gas–solid fluidized beds—Part II: freely bubbling gas–solid fluidized beds.* Chemical Engineering Science, 2005. **60**(1): p. 73-84.
7. Taghipour, F., N. Ellis, and C. Wong, *Experimental and computational study of gas-solid fluidized bed hydrodynamics.* Chemical Engineering Science, 2005. **60**(24): p. 6857-6867.
8. Busciglio, A., et al., *Analysis of the bubbling behaviour of 2D gas solid fluidized beds: Part II. Comparison between experiments and numerical simulations via Digital Image Analysis Technique.* Chemical Engineering Journal, 2009. **148**(1): p. 145-163.
9. Min, J., et al., *Experimental validation of CFD simulations of a lab-scale fluidized-bed reactor with and without side-gas injection.* AIChE Journal, 2010. **56**(6): p. 1434-1446.
10. Acosta-Iborra, A., et al., *Experimental and computational study on the bubble behavior in a 3-D fluidized bed.* Chemical Engineering Science, 2011. **66**(15): p. 3499-3512.
11. Chalermsinsuwan, B., P. Piumsomboon, and D. Gidaspow, *Kinetic theory based computation of PSRI riser: Part II-Computation of mass transfer coefficient with chemical reaction.* Chemical Engineering Science, 2009. **64**(6): p. 1212-1222.
12. Chalermsinsuwan, B., P. Piumsomboon, and D. Gidaspow, *A computational fluid dynamics design of a carbon dioxide sorption circulating fluidized bed.* AIChE Journal, 2010. **56**(11): p. 2805-2824.
13. Deng, Z., et al., *Numerical simulation of chemical looping combustion process with CaSO4 oxygen carrier.* International Journal of Greenhouse Gas Control, 2009. **3**(4): p. 368-375.
14. Jung, J. and I.K. Gamwo, *Multiphase CFD-based models for chemical looping combustion process: Fuel reactor modeling.* Powder Technology, 2008. **183**(3): p. 401-409.
15. Cloete, S., S.T. Johansen, and S. Amini, *An assessment of the ability of computational fluid dynamic models to predict reactive gas–solid flows in a fluidized bed.* Powder Technology, 2012. **215-216**(0): p. 15-25.
16. Cloete, S., S. Amini, and S.T. Johansen, *On the effect of cluster resolution in riser flows on momentum and reaction kinetic interaction.* Powder Technology, 2011. **210**(1): p. 6-17.
17. Cloete, S., et al., *Comparison of phenomenological and fundamental modelling approaches for predicting fluidized bed reactor performance.* Powder Technology, 2012. **228**(0): p. 69-83.
18. Cloete, S., S.T. Johansen, and S. Amini, *Investigation into the effect of simulating a 3D cylindrical fluidized bed reactor on a 2D plane.* Powder Technology, 2012. **Under review**.

19. Laverman, J.A., et al., *Investigation into the hydrodynamics of gas–solid fluidized beds using particle image velocimetry coupled with digital image analysis.* The Canadian Journal of Chemical Engineering, 2008. **86**(3): p. 523-535.
20. de Jong, J.F., M. van Sint Annaland, and J.A.M. Kuipers, *Experimental study on the effects of gas permeation through flat membranes on the hydrodynamics in membrane-assisted fluidized beds.* Chemical Engineering Science, 2011. **66**(11): p. 2398-2408.
21. Syamlal, M., W. Rogers, and T.J. O'Brien, *MFIX Documentation: Volume 1, Theory Guide.* 1993, Springfield: National Technical Information Service.
22. Van Wachem, B.G.M., et al., *Comparative analysis of CFD models of dense gas-solid systems.* AIChE Journal, 2001. **47**(5): p. 1035-1051.
23. Gidaspow, D., R. Bezburuah, and J. Ding, *Hydrodynamics of Circulating Fluidized Beds, Kinetic Theory Approach*, in *7th Engineering Foundation Conference on Fluidization* 1992. p. 75-82.
24. Schaeffer, D.G., *Instability in the Evolution Equations Describing Incompressible Granular Flow.* Journal of Differential Equations, 1987. **66**: p. 19-50.
25. Ogawa, S.U., A.; Oshima, N., *On the Equation of Fully Fluidized Granular Materials.* Journal of Applied Mathematics and Physics, 1980. **31**: p. 483.
26. Johnson, P.C. and R. Jackson, *Frictional-Collisional Contitutive Relations for Granular Materials, with Application to Plane Shearing.* Journal of Fluid Mechanics, 1987. **176**: p. 67-93.
27. Patankar, S., *Numerical Heat Transfer and Fluid Flow*. 1980: Hemisphere Publishing Corporation.
28. Leonard, B.P. and S. Mokhtari. *ULTRA-SHARP Nonoscillatory Convection Schemes for High-Speed Steady Multidimensional Flow*. in *NASA TM 1-2568 (ICOMP-90-12)*. 1990. NASA Lewis Research Center.
29. Montgomery, D., *Design and Analysis of Experiments*. 5 ed. 2001, New York: John Wiley and Sons.
30. Mostoufi, N., H.P. Cui, and J. Chaouki, *A comparison of two- and single-phase models for fluidized-bed reactors.* Industrial & Engineering Chemistry Research, 2001. **40**(23): p. 5526-5532.